Electrochemical Studies on $LaNi_{5-x}Sn_x$ Metal Hydride Alloys

B. V. Ratnakumar

Electrochemical Technologies Group, Jet Propulsion Laboratory

4800, Oak Grove Dr., Pasadena, California 91109

and

C. Witham, R. C. Bowman, Jr., A. Hightower, and B. Fultz

Division of Engineering and Applied Science

California Institute of Technology, Pasadena, California 91125

ABSTRACT

Electrochemical studies were performed on $LaNi_{5-x}Sn_x$ with $0 \leq x \leq 0.5$. We measured the effect of the Sn substituent on the kinetics of charge transfer and diffusion during hydrogen absorption and desorption, and the cyclic lifetimes of $LaNi_{5-x}Sn_x$ electrodes in 250 mAh laboratory test cells. We report beneficial effects of making small substitutions of Sn for Ni in $LaNi_5$ on the performance of the metal hydride alloy anode in terms of cyclic lifetime, capacity and kinetics. The optimal concentration of Sn in $LaNi_{5-x}Sn_x$ alloys for negative electrodes in alkaline rechargeable secondary cells was found to lie in the range $0.25 \leq x \leq 0.3$.

INTRODUCTION

The use of metal hydrides (MI]) as negative electrodes in alkaline rechargeable cells is becoming inci easingly popular, owi ng to advanta ges of the metal hydrides over convent ional anode materials (such as Zn, (d) in specific energy, cyclic lifetime and environmental compatibility. The similarities in the cell voltage, pressure characteristics and charge control methods of the Ni-MH cells to the commonly used Ni-Cd cell suggest that Ni-MH cells may take over a good fraction of the rechargeable battery market for consumer electronics in the nex t few years

Two classes of recta] hydride alloys currently being developed are those based on rare earth metals (AB_5)[1,2] and on early transition metals (AB_2)[3]. Although AB_2 alloys are reported to exhibit higher specific energy than the AB_5 alloys, state-of-the.a] t commercial Ni-MH cells predominantly use AB_5 al loys 'The AB_5 alloys are based on $LaNi_5$ with various substituents for La and Ni. The systematic effects of these alloy modifications, and the reasons for these effects, are active topics of research. An important goal of an alloy modification is to increase the lifetime of the MH electrode under cl~argc-discharge cycling. It has been found that the cyclic lifetime is affected by the alloy modifications, but it is not clear why. Impi oved cyc lic li fetimes with Co substitutions have been attributed to a reduced volume change upon hydrogen absorption and desorption.[1] Sakai,

et al [4] studied various ternary substitution for Ni in $LaNi_5$, and reported that the cyclic lifetime improves with the ternary substituents studied in the order Mn < Ni < Cu < Cr < Al < Co. It has also been suggested that the substitution of the rare earth metal with Ti[5], Zr[6] or other lanthanides such as Nd[7] and may promote the formation of a protective surface film and enhance the cyclic lifetime. This is auspicious for the use of relatively inexpensive misch metal, Mm (a naturally occurring mixture of rare earth metals La, Ce, Pr and Nd) for La in alloy formulations such as $(Mm)(Ni\text{-}Co\text{-}Mn\text{-}Al)_5$.[8,9]

The beneficial effect of the substituents for either La or Ni is often accompanied by an undesirable decrease in the hydrogen absorption capacity, long activation and slow kinetics of hydrogen absorption and desorption. In our recent communications,[10,11] we described the advantages associated with using Sn as a ternary substituent. The addition of small amounts (3.3 at%) of Sn improves the cycle life and the kinetics of absorption and desorption, with a marginal reduction in the specific capacity. The specific capacity of $LaNi_{4.8}Sn_{0.2}$ is about 300 mAh/g and is retained well during charge-discharge cycling. The benefits of alloying with Sn have also been realized in multi-component alloys.[12] In this paper, we present results from further studies on the Sn-modified $LaNi_5$ alloys of differing Sn concentrations. These studies were aimed at identifying the effect of the Sn additive on electrochemical characteristics of the metal hydride alloys, including the

kinetics of charge transfer and diffusion during the hydriding process, and cyclic lifetimes in 250 mAh laboratory test cells.

EXPERIMENTAL

The $LaNi_{5-x}Sn_x$ alloys were prepared by either arc-melting or induction-melting stoichiometric amounts of each metal Nickel (99.996), and Tin (99.999%) were obtained from Johnson Matthey, MA, USA, and Lanthanum (99.99(%) was obtained from Johnson Matthey, UK. The samples with x 0.4 & 0.5 originally produced by Hydrogen Consultants, inc., Littleton, CO were treated in the same manner as all other alloys, which were produced at Caltech. To insure homogeneous distribution of Sn in the alloys, the ingots were subsequently annealed in vacuum at 950°C for 72 hours. The annealed ingots were then crushed to 10 mesh in an argon glove box, followed by a single hydrogen absorption/desorption cycle to activate the alloys and to obtain alloy powders of optimized surface area. The chemical composition and homogeneity of the alloys were characterized by X-ray diffractometry. X-ray data were obtained with an INEL CPS-120 powder diffractometer using Co Kα radiation (λ = 1.7902 Å).

Pressure-composition isotherms were obtained for $LaNi_{5-x}Sn_x$ alloys by using a modified gas-manifold Sievert's apparatus described previously [13]. The electrode powder mixture

contained 76% MH alloy powder (< 75μm), 19% INCO nickel powder (1μm) as a conductive diluent, and 5% Teflon binder. The electrodes for the cyclic lifetime studies (area: 2.54 X 2.54 cm) were fabricated by hot-pressing at 150°C and 10,000 psi, approximately 1.3g of the mixture (1g MH powder) onto an expanded Ni screen. For the basic electrochemical studies, recessed cylindrical cavity BAS (Bio-Analytical Systems) disk electrodes were hand-packed with approximately 110mg of the electrode powder mixture (as in a paste electrode) to ensure consistent values for the electrode area (0.09 cm^2) and porosity. NiOOH electrodes from an aerospace Ni-Cd cell, supplied by Eagle-Picher, formed the counter electrode in each type of cell. A three-electrode flooded open cell with a Luggin capillary for the Hg/HgO reference electrode[14] was adopted for the basic electrochemical studies (basic cell). For the cyclic lifetime studies, the same components were assembled in a prismatic glass cell with nylon (Pellon 2516) separator. Teflon shims were used to provide adequate compaction to the electrodes. The electrolyte contained 31 w% KOH solution prepared with twice-distilled low-conductivity water. Although these were not sealed cells, a viton O-ring seal did enable the cells to reach pressure slightly above atmospheric conditions. Electrochemical measurements (DC) were performed with an EG&G 273 Potentiostat/Galvanostat interfaced to an IBM-PC, using EG&G Corrosion Software 252. AC impedance measurements were carried out with the EG&G 273 Potentiostat and Solartron 1255 Frequency Response Analyzer, using EG&G Impedance software 388. Cycling of the

prismatic cells was carried out with an automatic battery cycler made by Arbin Corp., College Station, TX. The cycling conditions include a discharging at a constant current of 12.5 mA/cm^2 (150 mA/g, C/2 rate) to -0.5 V vs. Hg/HgO. Charging at a constant current of 5 mA/cm^2 (60mA/g, C/5 rate) was performed to a charge return of 115% to ensure complete charging of the metal hydride electrode.

RESULTS AN I) DISCUSSION

X-RAY DIFFRACTOMETRY

X-ray diffractometry was used to characterize the. microstructure, measure the lattice parameters, and verify the phase composition of the MH alloy. Figure 1 shows the diffraction patterns of $LaNi_{5-x}Sn_x$ alloys with different Sn compositions, x. The X- ray diffraction patterns confirmed that alloys with Sn compositions up to x = 0.5 were entirely the (laO_3-type Haucke phase. With increasing Sn concentration, the diffraction peaks shift to smaller angles (as illustrated in the insert), implying an increase in the lattice parameters

ISOTHERMS

To understand the hydrogen absorption and desorption characteristics of the alloys, pressure-composition isotherms were measured. Such isotherms were obtained both in the gas phase and in the electrochemical environment. In addition, independent measurement of the gas-phase isotherms for several of these same alloys were made by Luo and co-workers.[15,16] Good agreement in the isotherms was found in all the cases.

Electrochemical (EC) isotherms were constructed from the equilibrium electrode potentials at different stages of hydrogen absorption or desorption. These are similar to coulometric titrations carried out on the battery electrode materials.[17] The equilibrium electrode potentials are related to the equilibrium hydrogen pressure,[18] P_{H_2}, by the Nernst equation:

$$E_o \text{ (vs. HgO/Hg)} \quad 0.9824 - 0.0291 \log(P_{H_2}) \qquad (1)$$

The EC isotherms differ slightly from the gas phase isotherms during absorption in that the inflection in the pressure at the end of absorption is absent, possibly because the internal pressures are limited to 1 atmosphere in the basic cell. The discharge isotherms, on the other hand, bear a greater resemblance to the gas phase isotherms. The plateau pressures calculated from EC isotherms during charge and discharge are generally comparable to those measured by gas phase isotherms. Figure 2 shows the EC isotherms during hydrogen absorption (charge) and desorption (discharge) of $LaNi_{5-x}Sn_x$ alloys with $0.1 \leq x \leq 0.3$, along with a representative gas-phase isotherm of $LaNi_5$. The changes in the

plateau pressures during absorption and desorption with a change in the Sn concentration are shown in Fig. 3.[19] It has been noted that increasing amounts of Sn induce a lattice expansion that is linear with Sn composition.[20,21,22] The logarithmic decrease in plateau pressure with increasing unit cell volume seen here is consistent with the observations of Gruen, et al.[23] As also shown in Fig. 3, the hysteresis between the absorption and desorption isotherms of $LaNi_5$ is reduced in the Sn-substituted alloys.

Hydrogen Absorption Capacity

The hydrogen absorption capacities of the $LaNi_{5-x}Sn_x$ alloys were measured both in the gas phase and electrochemical environments, as summarized in Fig. 4. Upon Sn substitution, the specific hydrogen absorption capacity calculated for $LaNi_{5-x}Sn_xH_6$ decreases marginally owing to the mass of Sn atoms. As the Sn composition increases, the intrinsic capacity, as measured in the gas phase[15,16,22] is increasingly smaller than these formula values. To determine the discharge capacity, all the electrodes were charged initially at 22 and 5 mA/cm^2 (22.8 and 60 mA/g) in the disk and prismatic electrodes respectively, to about 400 mAh/g. This overcharge of about 20-40% was used to ensure a complete hydriding of the electrodes. There is no inflection in the charge potentials at the end of charge owing to the hydrogen evolution reaction occurring at the same potentials.

After charging, the disk and prismatic electrodes were discharged at 44.4 and 12.5 mA/cm^2 (36.4 and 150 mA/g), respectively, to 1.5 V vs. 1 g/HgO. The discharge capacity improves significantly with the initial increase in Sn composition (Fig. 4). The disparity in measured capacities between basic and prismatic cells could result from a number of factors. The basic cell was limited to atmospheric pressure, while the prismatic cells were able to contain pressures slightly above atmospheric. The capacity for the basic cell is taken from the first cycle, while the prismatic value is taken at the maximum of the cyclic lifetime curve, implying incomplete MH powder activation in the disk electrodes. The disk electrodes were also thicker than those in the prismatic cells (3175 mm vs. ~1 mm) and experienced a larger current density per unit area. The electrochemical capacity of the binary alloy is particularly low during its charging, significant hydrogen evolution is observed to occur on its surface, which seems to be favored over hydrogen absorption. A similar difficulty in the charging of the binary alloy has been recently reported by Wasz et al., which they overcame by operating their cells at lower temperatures.[22] The maximum discharge capacity measured in prismatic cells was slightly over 300 mAh/g at a discharge rate of C/2, which is an impressive value for an AB_5 alloy. For example, some of the state-of-the-art, mischmetal-based AB_5 MH alloys evaluated at JPL showed a maximum capacity of 250-275 mAh/g.[24] Apart from the ease in chargeability, the low plateau pressures induced by the Sn substitution result in Ni-MH cells of low operating pressures and low self-discharge.

The discharge potentials decrease with an increase in the Sn concentration. This is expected from the reduced plateau pressure with increasing Sn concentration in the alloy. The charge potentials were lower than the equilibrium potentials calculated with Eq 1. However, the decrease in the electrochemical capacity of alloys with high Sn concentrations is significant compared to the decrease in the calculated capacity or the hydrogen absorption capacities measured with gas-phase isotherms. From an examination of the observed mid-point potentials taken from the dynamic discharge curves in the basic cell and the corresponding equilibrium potentials calculated from the desorption plateau pressures (Fig. 5), it is clear that the discharge overpotentials tend to increase at high Sn compositions, especially for $x > 0.3$. This behavior prompted us to carry out measurements on the kinetics of electrochemical hydriding of $LaNi_{5-x}Sn_x$ alloys.

Kinetics of Hydriding

DC Polarization

The kinetics of hydrogen absorption/desorption may be slowed by the alloy substituents. For example, elements forming surface films may alter the kinetics of charge transfer at, or transport of hydrogen through, the surface regions. To determine the effects of the partial substitution of Ni with Sn on the charge and discharge kinetics, DC polarization and AC

impedance experiments were performed on disk electrodes made with the MIJ alloys. Micropolarization and Tafel measurements were performed on the alloys under potentiodynamic conditions at scan rates of 0.02 mV/s and 0.5 mV/s, respectively. The scan rates were so chosen to provide near-steady state conditions with minimal changes in the state of charge of the electrode or its surface conditions. Although these tests were done in open cells, the results should be valid for sealed cells as well, because additional experiments on the x = 0.2 alloy have demonstrated that the kinetics as measured by micro- and Tafel polarization are fairly independent of the state of charge of the material.

Figure 6 shows the micropolarization curves of the $LaNi_{5-x}Sn_x$ alloys. These curves are reasonably linear and spread out owing to the difference in their equilibrium potentials. The potential of the binary alloy is less anodic (negative) than expected from the calculated equilibrium potentials. This may be caused by its lower state of charge in the unsealed cell configuration. The values of the exchange currents estimated from the slopes of micropolarization curves of different MIJ alloys show an interesting trend (Fig. 7 and Table I). The exchange current (i_0) increases initially upon Sn substitution from 0.77 mA for the binary alloy to 1.35 mA for the MIJ alloy with x = 0.1. Further addition of Sn decreases the exchange current. Nevertheless, the kinetics of Sn substituted alloys are superior to those of the binary alloy for Sn compositions of $x \leq 0.3$ in unsealed cells. With Sn compositions of $x \geq 0.4$, the kinetics of hydrogen absorption and desorption are

slowed considerably, and are even slower than in the binary alloy. The increases in the polarization resistance at higher Sn concentrations may be caused by an incomplete activation of the MH alloy, as discussed in the section on cyclic lifetimes.

To determine the kinetics of absorption and desorption, Tafel polarization measurements were made on the $LaNi_{5-x}Sn_x$ alloys. Figure 8 illustrates the Tafel behavior, corrected for mass transfer, of various alloys during charge and discharge. The overpotentials at any current density can be seen to decrease upon the initial substitution of Sn, but increase at the highest Sn concentration. The cathodic Tafel plot of the binary alloy is complicated by the hydrogen evolution reaction, which occurs at the same potentials as the hydriding reaction, resulting in two distinct slopes. The simultaneous occurrence of the hydrogen evolution may result in fluctuations in the electrode potentials from the continual forming and bursting of hydrogen gas bubbles on the electrode surface. Such problems are fortunately absent with Sn-substituted alloys, and the Tafel curves are more reproducible. In any case, for the Tafel polarization experiments, the potential was scanned from extreme anodic (positive) values to the cathodic (negative) values, to avoid the uncertainties arising from hydrogen bubbles adhering to the surface of the MH electrode.

The Tafel polarization curves indicate strong mass transfer effects at high currents. The limiting currents may be related to the slow solid-state diffusion of hydrogen in the MH

electrode. The limiting currents are measured in a separate potentiodynamic experiment at a potential 400 mV more positive than the equilibrium potential, and are listed in Table 1 The diffusion limiting current on discharge is highest for a Sn composition of $0.1 \leq x \leq 0.2$ (in the range of 500 mA/g) and is reduced at high Sn compositions. Using the measured limiting current, the Tafel plots can be corrected for the mass transfer effects by plotting the logarithm of $1/(1-1/1_{lim})$ against the electrode potential. The corrected Tafel plots are more linear (Fig. 8) The exchange current density and transfer coefficients for hydrogen absorption were calculated from the intercept and inverse slope of the corrected cathodic Tafel plots, respectively The corresponding coefficients for hydrogen desorption were calculated from the corrected anodic Tafel plots The absorption exchange current increases upon Sn substitution and shows a maximum at a Sn composition of $x = 0.2$ (Fig 7, Table I) The desorption exchange current improves more significantly upon Sn substitution, but has a maximum near $x = 0.1$. Nevertheless, the kinetics of desorption continues to be better than the binary alloy for $x < 0.4$. The Tafel slopes show an interesting trend the slope for the absorption process decreases with increasing Sn concentration, whereas the slope for the desorption process increases (Table 1). The change in both the parameters is less marked for $x > 0.2$ It is interesting to note that the equilibrium potentials (calculated from the logarithm of the plateau pressures) also decrease with increasing Sn concentration. It is known[2] that lower plateau pressures facilitate absorption, whereas higher plateau pressures are desirable for desorption. The

transfer coefficients during absorption calculated from the Tafel slopes increase with increasing Sn composition from O 24 for x 0 to 0.25, 0.32, 0.34, 0.35 and 0.4 for x values of 0,1, 0.2, 0,3, 0.4 and 0.5, respectively. The corresponding transfer coefficients during desorption, however, decrease with increasing Sn composition, from 0.55 for x = O to 0.32, 0.27, 0.28, 0.26 and 0.26

AC Impedance

1 lectrochemical Impedance Spectroscopy measurements were made on mixed anode. powders in the charged state. The powders were activated by gas-phase absorption but were not electrochemically cycled The AC impedance data were obtained in the frequency range of 100 kHz 105 mHz at a low AC amplitude of' 2 mV. The impedance plots of $LaNi_{5-x}Sn_x$ alloy electrodes are shown in the Nyquist or Cole-Cole form in Fig. 9. As may be seen in this figure, the impedance decreases noticeably upon initial substitution of Sn but increases for x . 0 1. '1 he impedance data were analyzed using a generalized equivalent circuit adopted for the MI] electr o(1c,[25] shown in the insert. The capacitive components labeled by Q are modeled as constant-phase elements (CPE) to describe the ,depressed nature of the semi-circles.[26] R_1 is ascribed to the electrolyte resistance between the MI] electrode and the reference electrode. The semi-circle in the high frequency region, represented by 1{, and Q_2, results from the contact resistance

between the current collector and the teflon bonded electrode. The contact resistance and capacitance between the particles of the plastic-bonded metal hydride powder, generate parameters R_3 and C_3. The semicircle in the low frequency region, modeled by R_4 and Q_4, is attributed to the reaction (charge transfer) resistance and the double-layer capacitance, respectively. The diffusional impedance, W_4, is the Warburg impedance, which is a parallel and/or series combination of diffusional resistance and pseudo-capacitance. The observed impedance patterns of the MA_{1-x} electrodes (Fig. 9) are simplified by the absence of a diffusional component. The parameters in the equivalent circuit were calculated by a non-linear least-squares fit using the Boukamp method.[27]

The exchange current calculated from the charge transfer resistance decreases initially upon the substitution of Sn but increases for Sn compositions $x \geq 0.4$ (Table 1). The trend is similar to that observed in the DC polarization experiments. It is thus clear that the kinetics of hydriding improves markedly upon Sn substitution in $LaNi_{5-x}Sn_x$, at least for $x \leq 0.3$. Higher amounts of Sn seem to cause sluggish kinetics for hydrogen absorption and desorption. This behavior is currently being studied in more detail.

Cyclic Lifetime

Finally, the performance of the MH alloys during charge-discharge cycling was evaluated in 250 m Ah, negative-limited, prismatic laboratory test cells. Although sealed cells are typically positive-limited in order to utilize an overcharge mechanism, the present partially sealed cells were designed in the negative-limited configuration (with a deficit of MH) to investigate the life-limiting mechanisms of the MH electrode. The cyclic lifetimes under these accelerated test conditions are expected to be shorter than in sealed commercial cells, but these tests should be appropriate for comparative evaluation of cyclic lifetimes of different metal hydride electrode materials with plateau pressures slightly greater than atmospheric, or less.

The cyclic lifetime of cells containing $LaNi_{5-x}Sn_x$ metal hydride alloys are presented in Fig. 10. This figure shows that the initial capacity increases with an increase in the Sn composition]." We attribute the lower capacities of the Sn-poor alloys to their high plateau pressures, which were around 1 atm. Since our cells operated only slightly above 1 atm., incomplete charging is expected for the alloys with $x < 0.2$. However, the initial capacity declines again for Sn concentrations higher than 6.7 at%, or $x \geq 0.4$. While suppressed hydrogen absorption/desorption kinetics could also be responsible for this trend at high Sn concentrations, we attribute this effect to the loss of intrinsic capacity of the alloy, incomplete activation, and the low desorption pressures of the alloys. As evident in

Figure 4, Sn compositions of $0.2 \leq x \leq 0.3$ provide the highest initial capacities of approximately 300 mAh/g.

It may be noted that our alloys all experience a shorter cyclic lifetime than those achieved by other experimenters,[12,22] and this can be attributed to the strenuous cycling conditions used to test our cells. The deep discharge to -0.5V vs Hg/HgO accelerates the loss in capacity,[4] compared to the -0.7V mentioned.[12,22] The high applied current density, normalized by area, and the large proportion of active material used in the electrode powder mixture contribute to the effective current density experienced by the MH powders being very large. We believe that these factors represent more accurately the lifetime the MH alloys will obtain in cells manufactured for consumer use.

Each cell was subjected to 200 charge-discharge cycles. The retention of capacity was found to improve with increasing Sn composition. After 100 charge-discharge cycles, alloys with $x = 0.25$ or 0.3 exhibit capacities in excess of 200 mAh/g, an impressive number when compared to the state of the art $MmNi_{3.5}Co_{0.8}Mn_{0.4}Al_{0.3}$ MH alloys evaluated at JPL[24] (M m in Fig. 10). It is interesting to note that alloys with high Sn compositions ($x \geq 0.4$) show long activation cycles, taking longer to achieve maximum capacity than alloys with $x \leq 0.3$. This was confirmed by activating a sample with $x = 0.4$ by thermally cycling it with hydrogen 5 times before electrochemical cycling. Data from this sample

are labeled as 0.4a in Fig 1 0. This sample was used for the capacity measurement in shown in Fig 4, but the curve in Fig 10 labeled 0.4 should be used to study the capacity degradation. We are currently studying in more detail how incomplete activation affects the alloys' charge/discharge kinetics, but the ~~lc.sent lc.suits should be valid for powders with a single gas-phase activation, The lifetime capacity in cells with x ? 0.4 exceeds that of cells with $0.2 \leq x \leq 0.3$, as evidenced by the lifetime curves after 150 cycles,

CONCLUSIONS

The substitution of small amounts of Sn for Ni in $LaNi_5$ improves many characteristics of the metal hydride anode in partially sealed prismatic alkaline rechargeable cells. Specifically, the chargeability is improved owing to reduced absorption plate.au pressures. The hydrogen absorption capacity of the $LaNi_{5-x}Sn_x$ alloys exceeds 300 mAh/g, an impressive number for an AB_5 formulation The kinetics of hydrogen absorption and desorption are improved markedly compared to the binary alloy, although at high Sn concentrations the improvement is less evident, possibly resulting from incomplete activation. The capacity retention during charge-discharge cycling is significantly enhanced such that the cyclic lifetime of Sn substituted alloys is comparable to some multi-component, Jnisch-metal based alloys '1 he compositions in the range of $0.2 \leq x \leq 0.3$ appear to be optimal for high capacities, long cyclic lifetime and improved kinetics. We suggest that higher Sn compositions ($0.4 \leq x \leq 0.5$) may be favored for high

temperature applications The simple alloy chemistry and absence of Co in these alloys gives them an advantage over the $MmNi_5(NiCoMnAl)_5$ alloys now being produced commercially.

ACKNOWLEDGMENTS

This work was carried out at the Jet Propulsion Laboratory under contract with the National Aeronautics and Space Administration and at the California Institute of Technology under funding by the DOE grant DE-FG03-94ER14493. We thank L. A. Wade of JPL for providing samples of several alloys and Prof. T. B. Flanagan of Univ. of Vermont, for supplying detailed results of their isotherm measurements.

REFERENCES

1 J. J. G. Willems, *Philips J. Res.*, 39 (Suppl. 1), 1 (1984); J J G. Willems and K. H. J. Buschow, *J. Less Common Metals* 129 13 (1987).

2 T. Sakai, K. Muta, H. Miyamura N Kuriyama and H Ishikawa, *Proc. Symp. Hydrogen Storage Materials, Batteries, and Electrochemistry*, 1 ECS Proc. Vol. 92-5, p.59 (1992); T. Sakai, H. Yoshinaga, H Miyamura and H Ishikawa, *J. Alloys and Compounds*, 180, 37 (1992)

3 S, R Ovshinsky, M. A. Fetcenko and J Ross, *Science*, ?60, 1 '/6 (1993); M. A. Fetcenko, S. Venkatesan and S R Ovshinsky, *Proc. Symp. Hydrogen Storage Materials : Batteries and Electrochemistry*, ECS Proc. Vol. 92-5, p. 141(1992); M. A. Fetcenko, S. Venkatesan, K C. Hong and B. Reichman, *Power Sources*, Vol. **12**, p. 411 (1988).

4. 'I'. Sakai, K. Oguru, H. Miyamura, N Kuriyama. A. Kato and H. Ishikawa, *J. Less-Common Metals*, **161,** 193 (1990)

5. T. Sakai, H. Miyamura, N. Kuiyama, A. Kato and K. Oguru *J. Less-Common Metals*, **1**S9, 1 ?.7 (1990)

6. 'I'. Sakai, H. Miyamura, N. Kuriyama, A. Kato, K. Oguiu and H. Ishikawa, *J. Electrochem.* Sot., **137**, 795 (1990)

7. '1'. Sakai, T. Hazama, H. Miyamura, N Kuriyama, A. Kato and 11 Ishikawa, *J. Less-Common Metals*, 172-174, 1175 (I 991)

8. N. Furukawa (Sanyo Electric Co.), *J. Power Sources*, **51**(1-2) 45 (1994)

9. K. Suzuki, N. Yanagihara, H. Kawano, A Ohta, (Matsushita, Japan), *J. Alloys and Compounds*, 192>173 (1993)

10. B. V. Ratnakumar, G. Halpert, C. Witham and B. Fultz, *J. Electrochemical Soc.*, **141**, 189 (1994).

11. B. V. Ratnakumar, S. Surampudi, S. Di Stefano, G. Halpert, C. Witham, A. Hightower and B. Fultz, *Proc. ECS Symp. Hydrogen Batteries*, Miami Beach, FL. **94-27**, 57 (1994).

12. A. Anani, A. Visintin, K. Petrov and S. Srinivasan, *J. Power Sources*, **47**, 261 (1994); M. P. S. Kumar et. al., *J. Electrochemical Soc.*, **142**, 3424 (1994).

13. R. C. Bowman, Jr., C. H. Luo, C. C. Ahn, C. K. Witham and B. Fultz, *J. Alloy Compounds*, **217**, 185 (1995).

14. B. V. Ratnakumar, S. Di Stefano, S. Surampudi and G. Halpert, *J. Electrochem. Soc.*, (in press).

15. S. Luo, W. Luo, J. D. Clewley, T. B. Flanagan and R. C. Bowman, *J. Alloy Compounds*, **231**, 473 (1995).

16. S. Luo, W. Luo, J. D. Clewley, T. B. Flanagan and L. A. Wade, *J. Alloy Compounds*, 231, 467 (1995).

17. For example, A. Anani and R. A. Huggins, *J. Power Sources*, **38**, 363 (1992).

18. C. Jordy, A. Percheron-Guegan, J. Bouet, P. Sanchez, C. Chanson and J. Leonardi, *J. Less Common Metals*, **172-174**, 1236 (1991).

19. Personal communication with T. B. Flanagan.

20. M. Mendelsohn, D. Gruen, A. Dwight, *Inorg. Chem.* **18**, 3343 (1979).

21. J. S. Cantrell, T. A. Beiter and R. C. Bowman, Jr., *J. Alloys and Compounds*, **207/208**, ***.37? (1994),***

22. M. Wasz, R. B. Schwarz, S. Srinivasan and M. P. S. Kumar, *1995 Spring MRS Symposium Proceedings on "Materials for Electrochemical Energy Storage and Conversion - Batteries, Capacitors, and Fuel Cells"*, 1995, in press.

23. D. N. Gruen, M. H. Mendelsohn and A. E. Dwight, *J. Less Common Metals*, **63**, 193 *(1979).*

24. B. V. Ratnakumar, S. Surampudi, S. Di Stefano and G. Halpert, *Proc. 36th Power Sources Conf.*, Cherry Hill, NJ, June (, 9) WI),

25. N. Kuriyama, T. Sakai, 11 Miyamura, I Uehara and 11, Ishikawa, *J. Alloys and Compounds*, 192,161 (1993)

26. J. Ross McRonald, *Impedance Spectroscopy*, John Wiley & Sons, NY (1987).

27.11. A. Boukamp, *Solid State Ionics*, 20, 31 (1986).

FIGURE CAPTIONS

Fig. 1: X-ray diffraction patterns of $LaNi_{5-x}Sn_x$ alloys. The inset shows the diffraction peaks shifting to smaller angles with increasing Sn composition.

Fig. 2: p-c-T isotherms of $LaNi_{5-x}Sn_x$ alloys. Electrochemical (○,● x = 0.3; ◊,♦ x = 0.2; □,■ x = 0.1; open - charge, closed . discharge) and gas-phase (- x=0.0)

Table 1: Exchange current densities of $LaNi_{5-x}Sn_x$ alloys, determined by electrochemical methods.

	M					m	
		i_o [mA]		Slope [mV/dec]		Current	
	i_o [mA]	Abs.	Des.	Abs.	Des.	[mA]	i_o [mA]
							2
			4.99	233	83		1.54
					210	334.7	1.15
							0.51
				229		265.6	0.52

Fig 3: Variation with the Sn composition in $LaNi_{5-x}Sn_x$ alloys of unit cell volume (□) and plateau pressure for 300 K absorption (○) and desorption (●).

Fig 4 Hydrogen absorption capacity of $LaNi_{5-x}Sn_x$ alloys measured with Sieverts' apparatus, prismatic cell electrode, disk electrode, and formula capacity for H/M ratio of 1:1.

Fig 5: Variation of mid-point discharge potentials of disk electrodes and the corresponding equilibrium potentials calculated from the desorption plateau pressures,

Fig 6 Linear polarization curves of $LaNi_{5-x}Sn_x$ alloys.

Fig 7: Variation of the exchange current density from measurements by DC micropolarization (■), AC Impedance (×), Anodic Tafel polarization (*) and Cathodic Tafel polarization (---).

Fig. 8: Tafel polarization curves with mass transfer corrections of $LaNi_{5-x}Sn_x$ alloys.

Fig. 9 Electrochemical Impedance Spectroscopy (EIS) curves of $LaNi_{5-x}Sn_x$. Insert shows equivalent circuit

Fig. 10: Cyclic lifetime behavior of $LaNi_{5-x}Sn_x$ alloys with comparison to the best Misch-metal based, multi-component alloy evaluated at JPL (ref. 24)

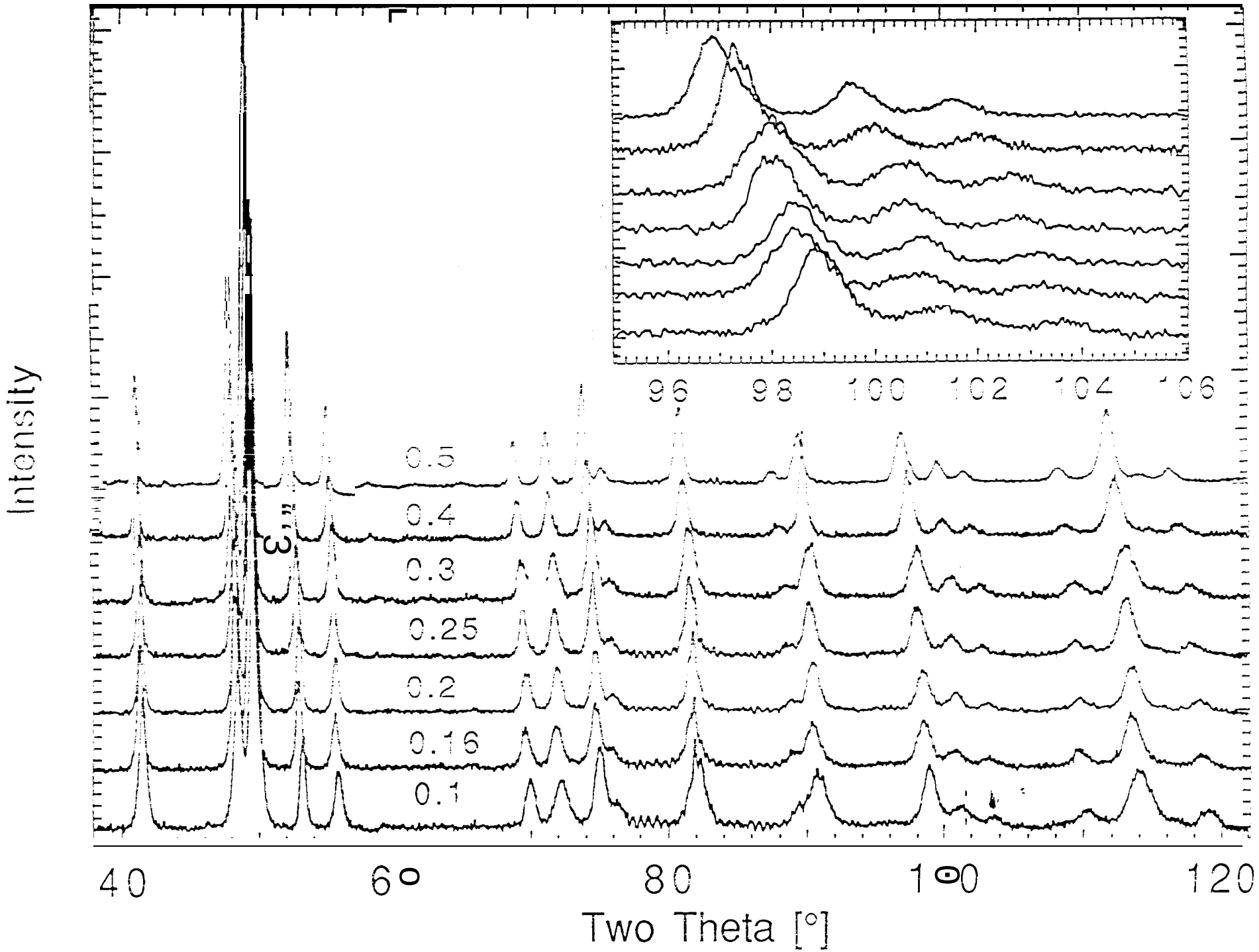

B. V. Ratnakumar, et al.

Figure 1

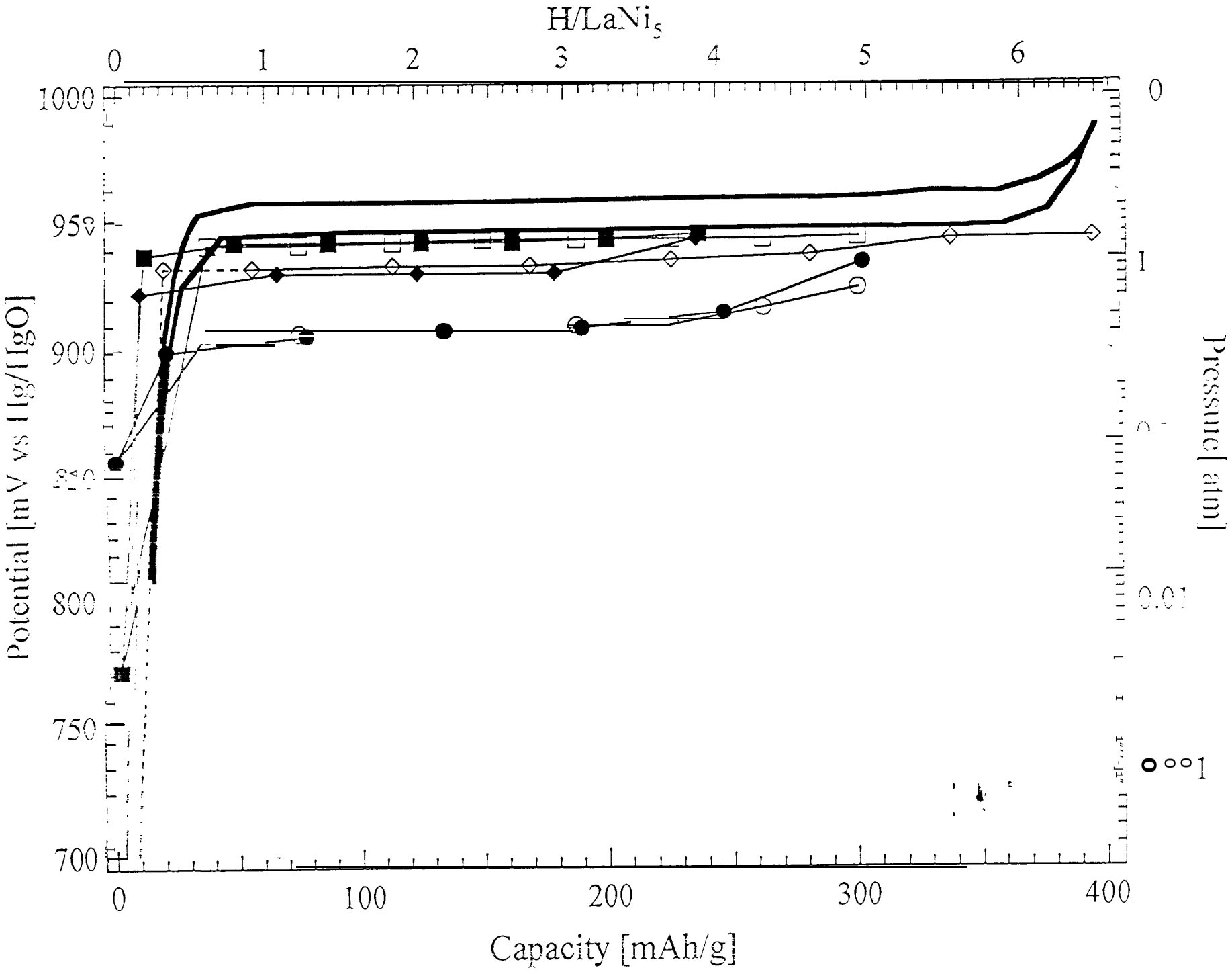

B. V. Ratnakumar, et al

Figure 2

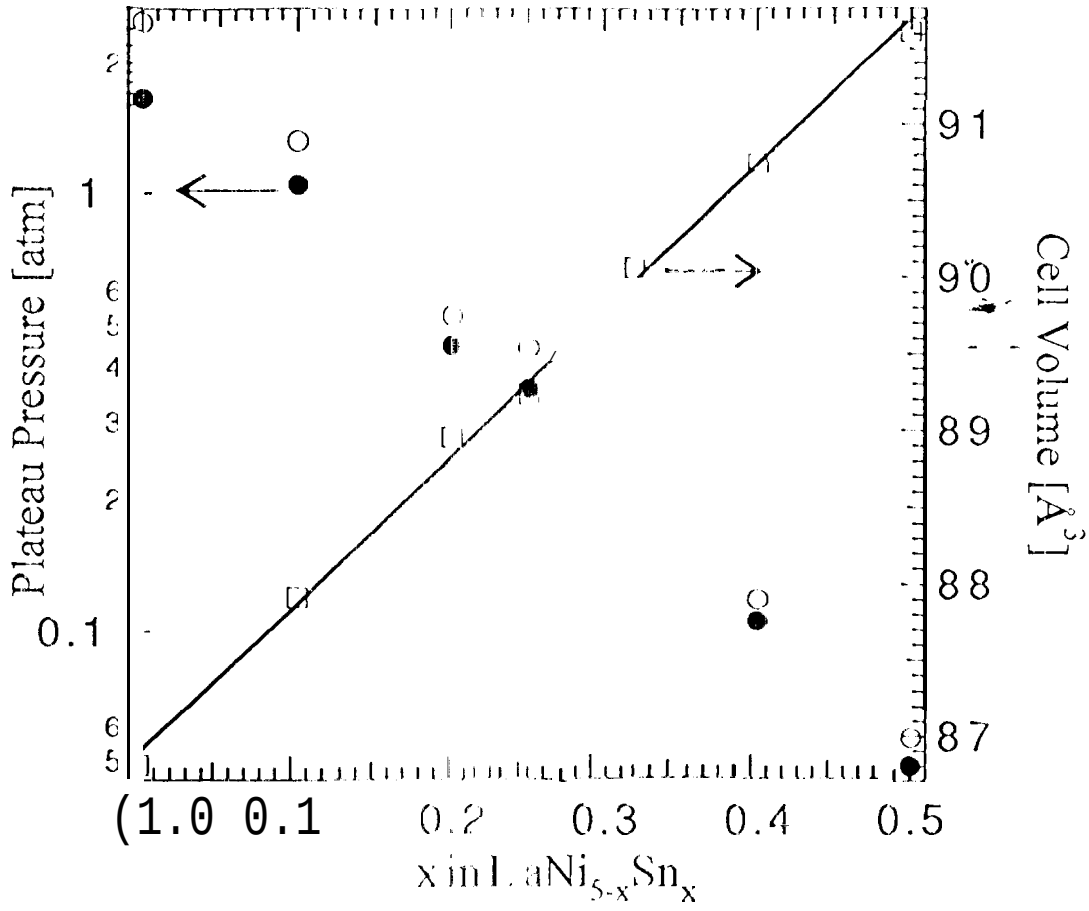

B. V. Ratnakumar, et al

Figure 3

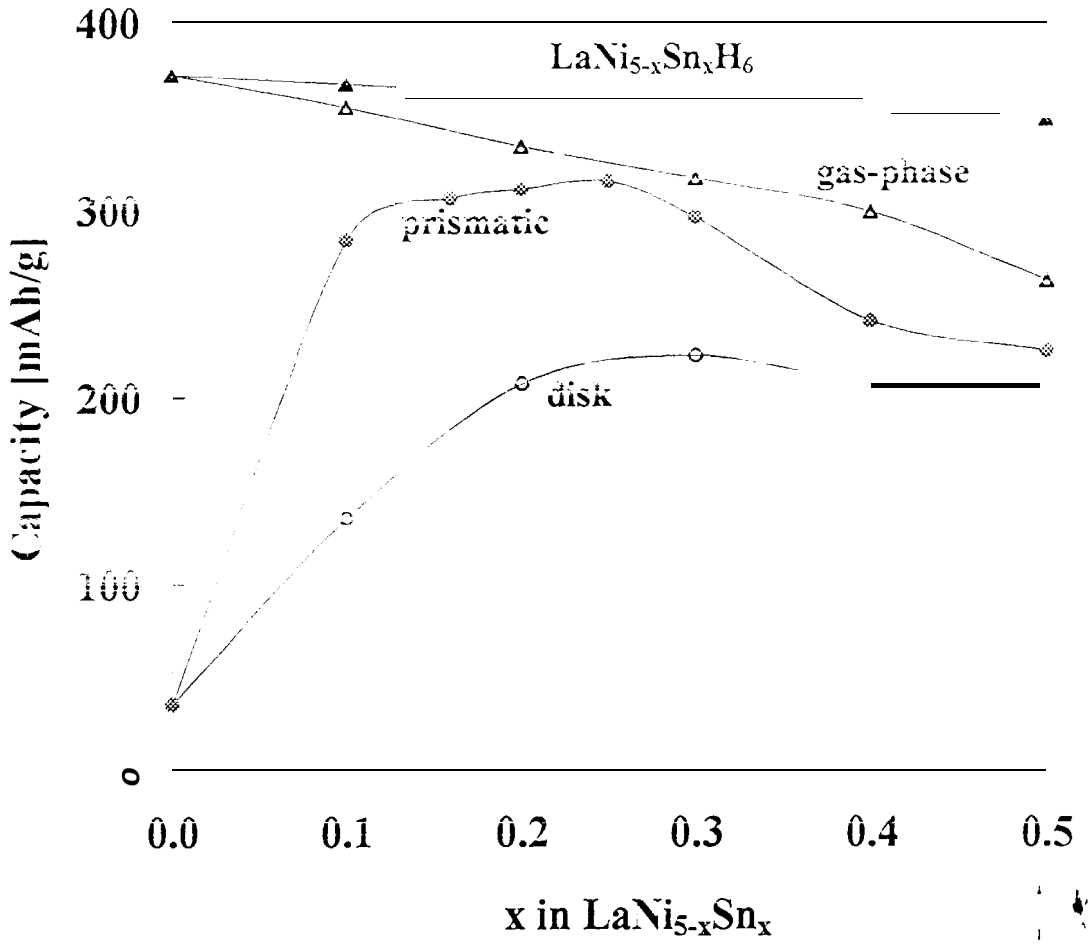

B. V. Ratnakumar, et al.

Figure 4

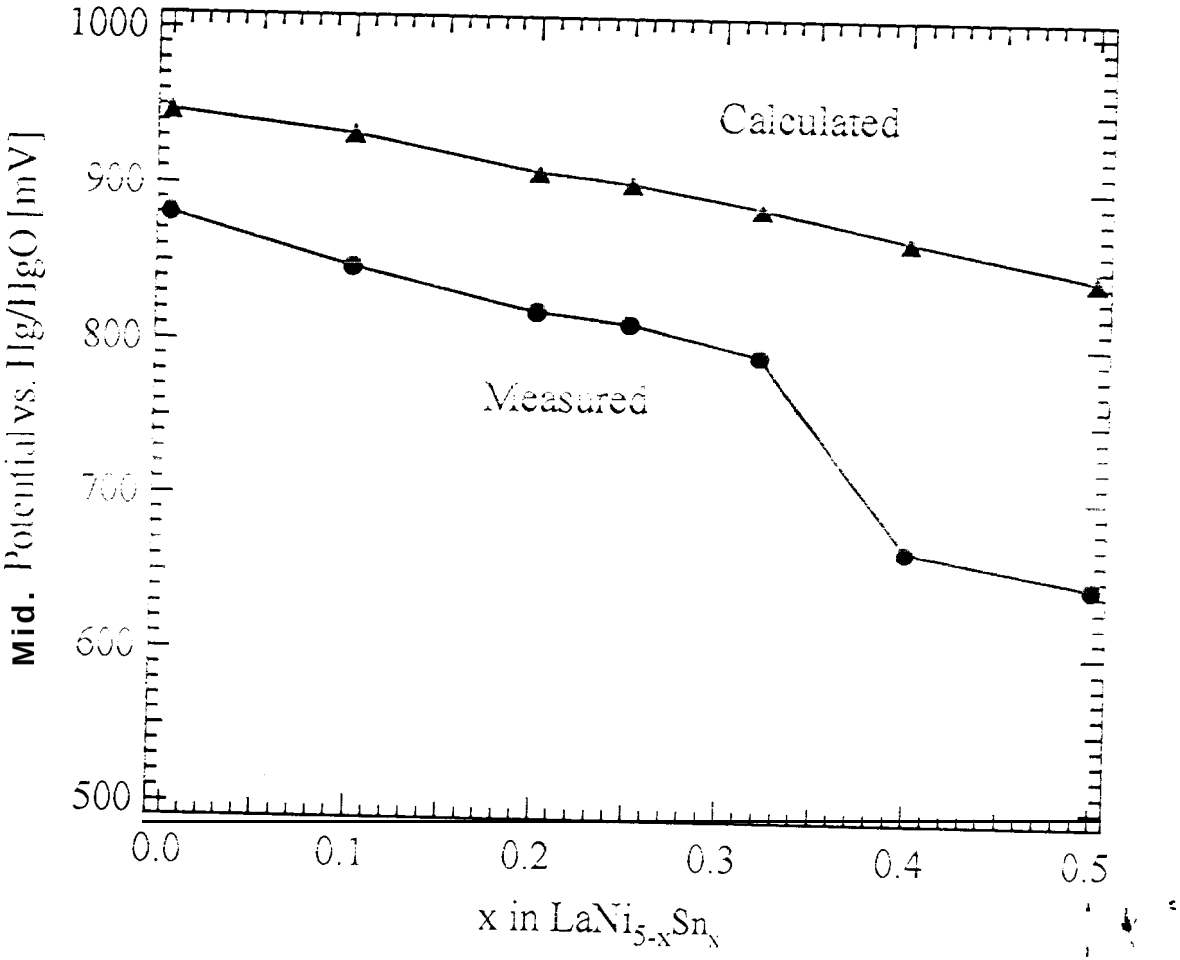

B V Ratnakumar, et al

Figure 5

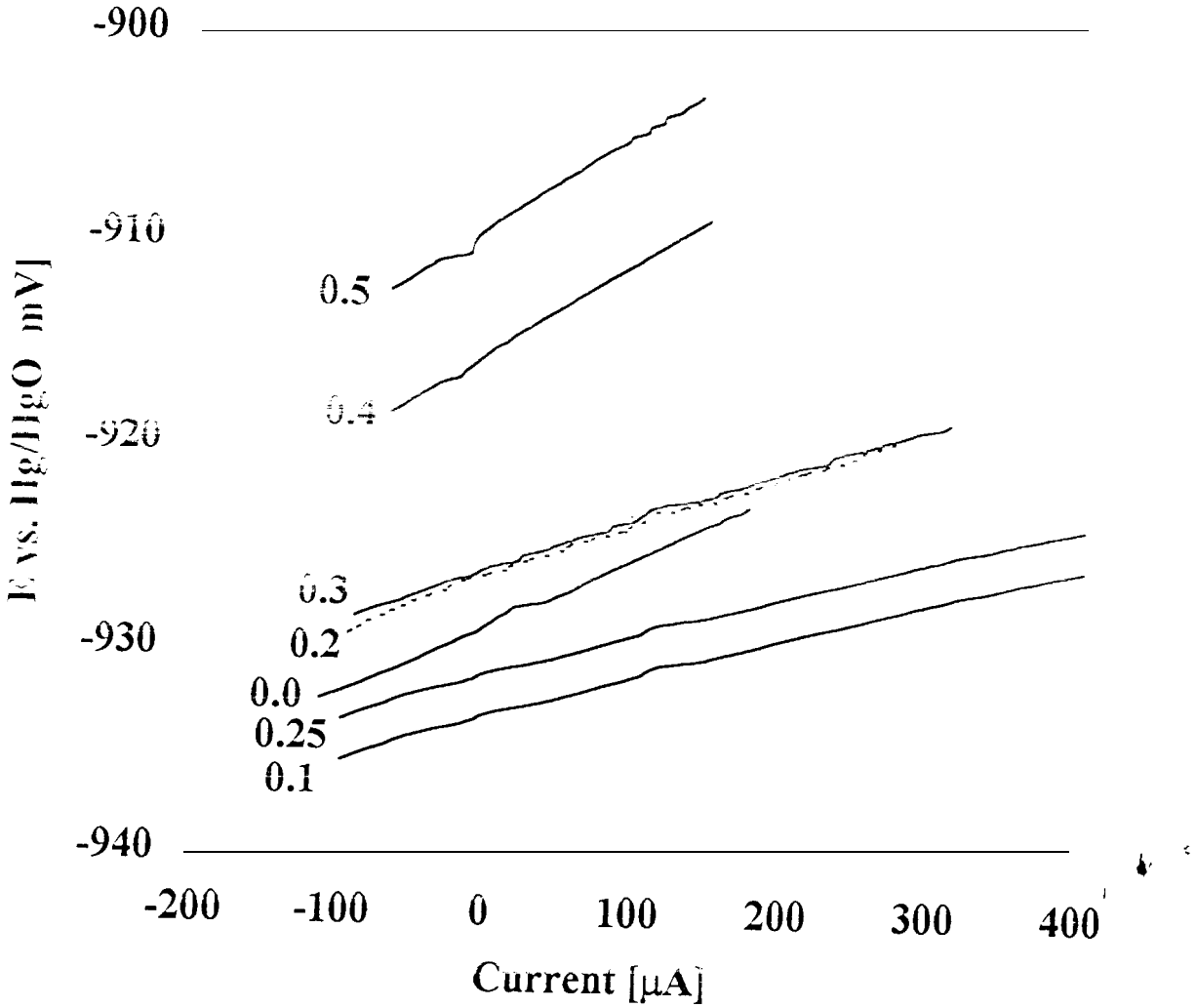

B V. Ratnakumar, et al.

Figure 6

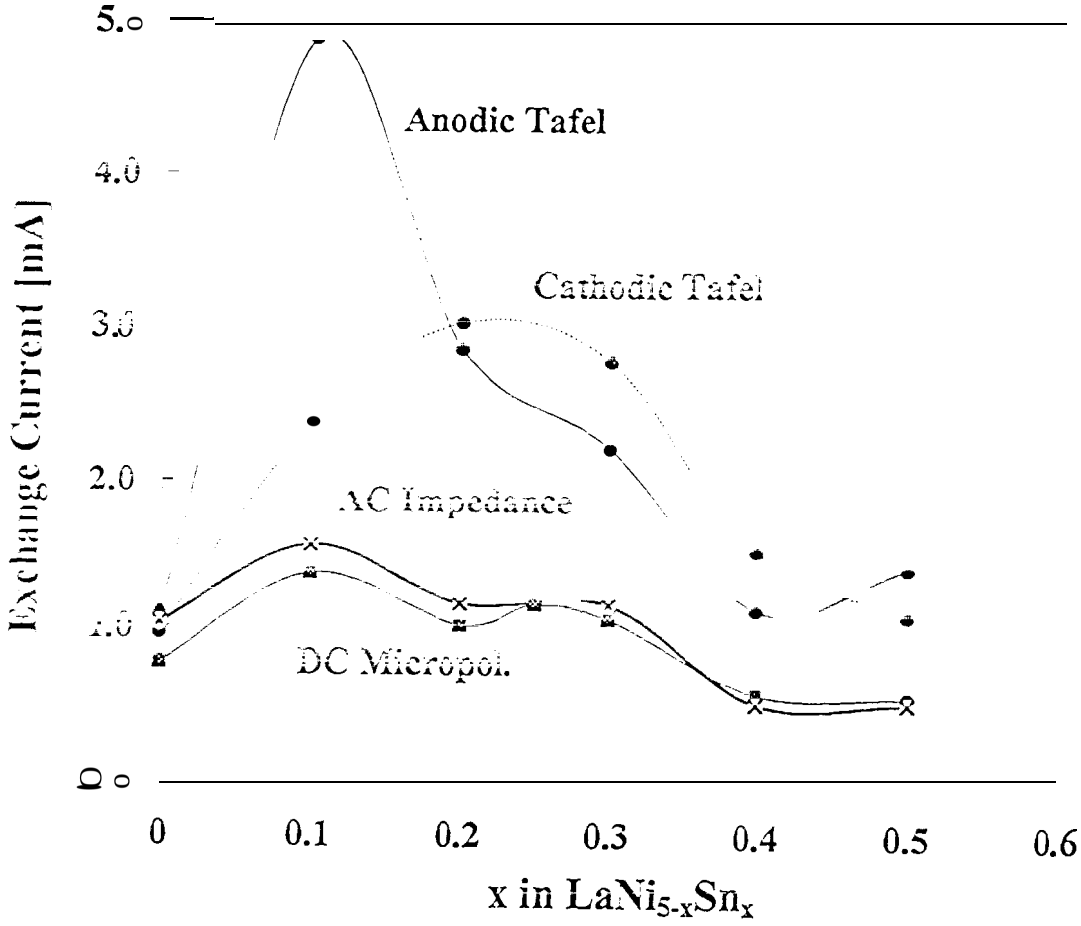

B. V. Ratnakumar, et al.

Figure 7

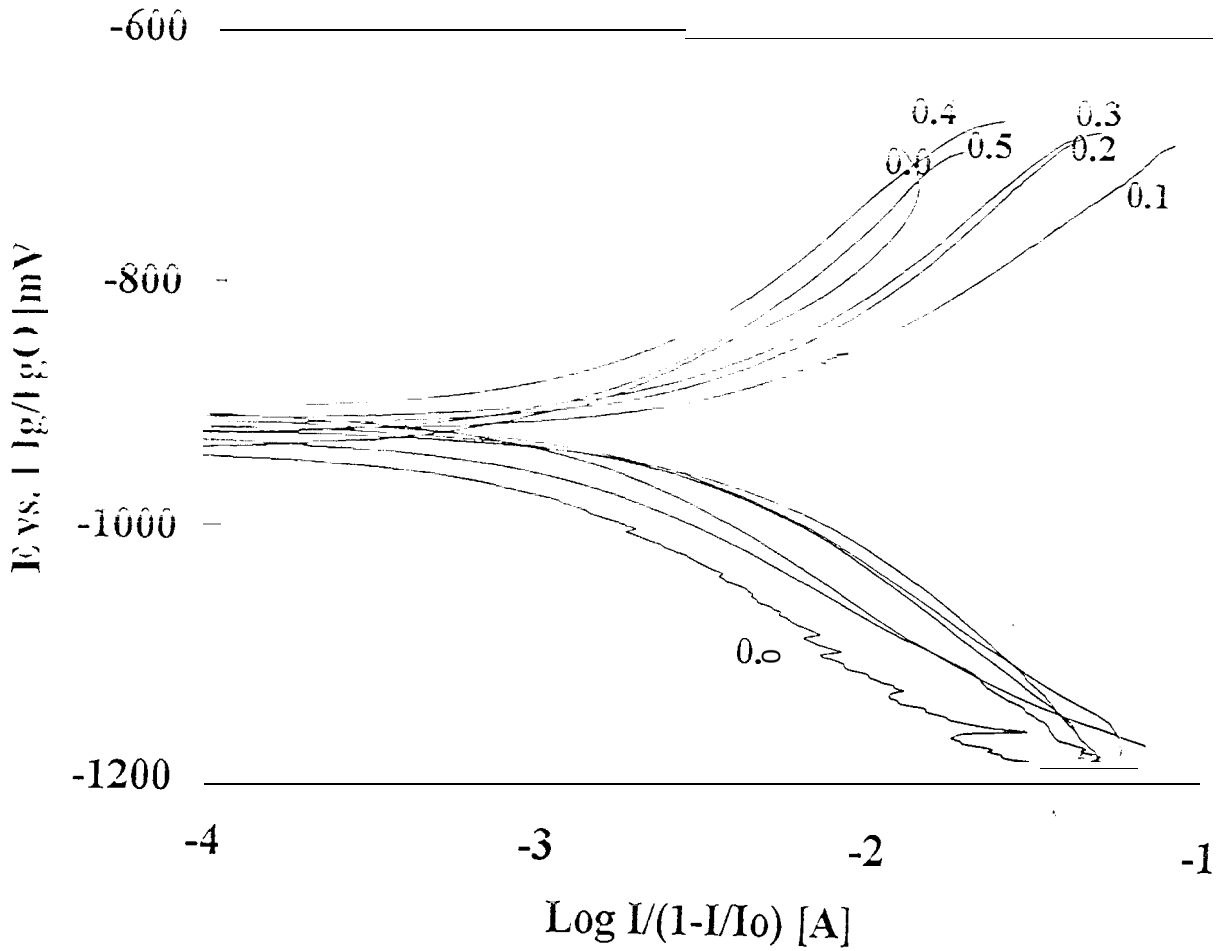

B V Ratnakumar, et al.

Figure 8

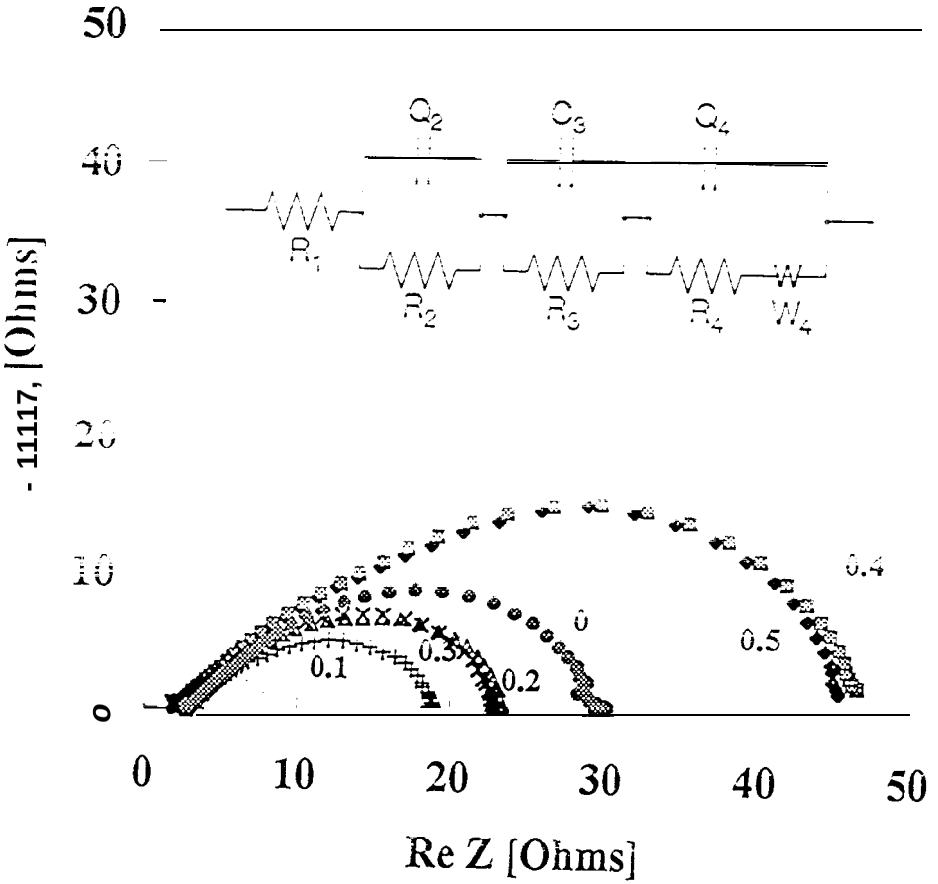

W. V. Ratnakumar, et al.

Figure 9

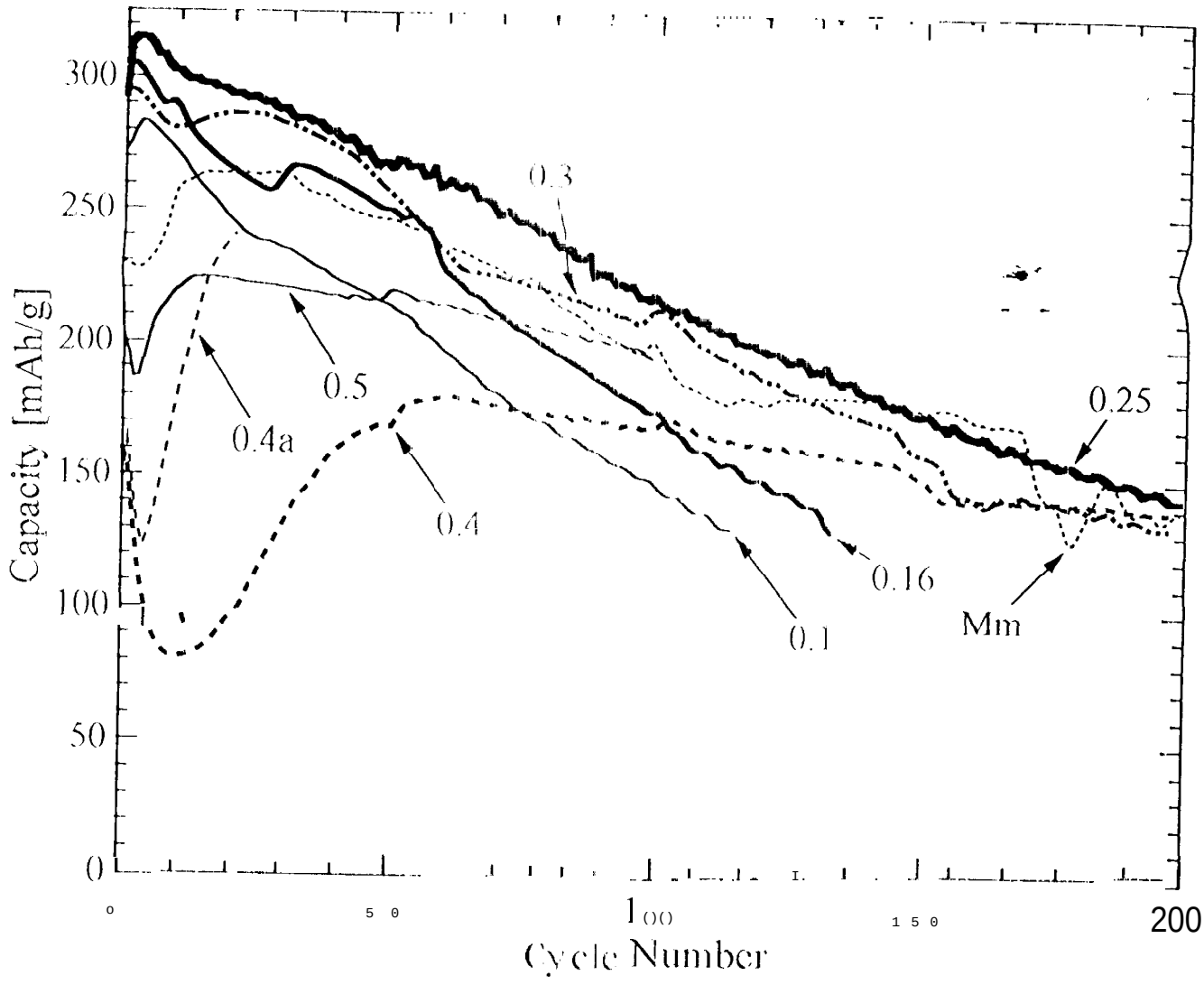

B. V. Ratnakumar, et al

Figure 10